Triphenylphosphonium-Conjugated Poly(ε-caprolactone)-Based Self-Assembled Nanostructures as Nanosized Drugs and Drug Delivery Carriers for Mitochondria-Targeting Synergistic Anticancer Drug Delivery

*Dong Youl Cho, Hana Cho, Kiyoon Kwon, Minjong Yu, Eunji Lee, Kang Moo Huh, Don Haeng Lee, and Han Chang Kang**

For mitochondria-targeting delivery, a coupling reaction between poly(ε-caprolactone) diol (PCL diol) and 4-carboxybutyltriphenylphosphonium (4-carboxybutyl TPP) results in the synthesis of amphiphilic TPP-PCL-TPP (TPCL) polymers with a bola-like structure. In aqueous environments, the TPCL polymer self-assembled via cosolvent dispersion and film hydration, resulting in the formation of cationic nanoparticles (NPs) less than 50 nm in size with zeta-potentials of approximately 40 mV. Interestingly, different preparation methods for TPCL NPs result in various morphologies such as nanovesicles, nanofibers, and nanosheets. In vitro cytotoxicity results with TPCL NPs indicate IC_{50} values of approximately 10–60 μg mL^{-1}, suggesting their potential as anticancer nanodrugs. TPCL NPs can be loaded both with hydrophobic doxorubicin (Dox) and its hydrophilic salt form (Dox·HCl), and their drug loading contents are approximately 2–10 wt% depending on the loading method and the hydrophilicity/hydrophobicity of the drugs. Although Dox·HCl exhibits more cellular and nuclear uptake, resulting in greater antitumor effects than Dox, most drug-loaded TPCL NPs exhibit higher mitochondrial uptake and approximately 2–7-fold higher mitochondria-to-nucleus preference than free drugs, resulting in superior (approximately 7.5–18-fold) tumor-killing activity for most drug-loaded TPCL NPs compared with free drugs. In conclusion, TPCL-based nanoparticles have potential both as antitumor nanodrugs themselves and as nanocarriers for chemical therapeutics.

1. Introduction

Interest in targeting drug delivery, which can specifically deliver payloads to sites of interest such as organs, tissues, cells, and subcellular organelles, is continuously growing because such a delivery strategy may facilitate greater accumulation of the delivered drugs at target sites and less accumulation at unwanted sites, which can then result in enhanced therapeutic efficacy and reduced undesirable effects.[1] Most targeting nanocarriers have been investigated at the cellular level because certain cells can express specific receptors or antigens, which can be specifically recognized and interact with their counterpart ligands or antibodies, on their plasma membrane.[2] However, although the majority of the delivered drugs may be delivered into specific cells, their enhanced therapeutic efficacy cannot be ensured because their action sites for generating therapeutic effects occur not just at the cellular level but at the subcellular level as well, for example, the cytosol, the nucleus, and the mitochondria.[2b] Thus,

D. Y. Cho, H. Cho, K. Kwon, Prof. H. C. Kang
Department of Pharmacy and Integrated Research Institute of Pharmaceutical Sciences
College of Pharmacy
The Catholic University of Korea
43 Jibong-ro, Wonmi-gu, Bucheon-si, Gyeonggi-do 420-743 South Korea
E-mail: hckang@catholic.ac.kr
M. Yu, Prof. E. Lee
Graduate School of Analytical Science and Technology
Chungnam National University
99 Daehak-ro, Yuseong-gu, Daejeon 305-764, South Korea
Prof. K. M. Huh
Department of Polymer Science and Engineering
Chungnam National University
99 Daehak-ro, Yuseong-gu, Daejeon 305-764, South Korea
Prof. D. H. Lee
Division of Gastroenterology and Hepatology
Department of Internal Medicine
Inha University Hospital
27 Inhang-ro, Jung-gu, Incheon 400-712, South Korea
Prof. D. H. Lee
Utah-Inha Drug Delivery Systems and Advanced Therapeutics Research Center
9 Songdomirae-ro, Yeonsu-gu, Incheon 406-840, South Korea

DOI: 10.1002/adfm.201501422

recently, subcellular targeting drug delivery systems that specifically reach subcellular compartments of interest have garnered attention.[2b,3]

Among various subcellular organelles, we have focused on mitochondria-targeting nanosystems. Mitochondria are very significant intracellular organelles that control the homeostasis of vital physiological functions (e.g., signaling, cellular differentiation, cell viability/apoptosis, cell cycle, cell growth, intracellular Ca^{2+} levels, and oxidative stress) and synthesize bioenergy molecules (e.g., ATP).[4] Their dysfunction leads to a variety of human disorders including neurodegenerative, neuromuscular, cardiac, and metabolic diseases.[4b],[5] To selectively deliver therapeutics into the mitochondria, mitochondria-targeting signal (MTS) peptides and lipophilic cations have been investigated.[5] Most studied MTS peptides (e.g., MSATRMQLLSPRNVRLLSRGRSELFAGGSGGGPRVRSLISP PLSSSSPGRALSSVSATRRGLPKEKMTENGVSSRAKVLTIDT,[6] MLSRAVCGTSRQLAPALGYLGSRQ,[7] MLSCTSPLLRGACH-NMGAAKALRLRWTVPPAVLIALGSGALY TTSGQTLYYK-NSVQQTD,[8] and MLFNLRILLNNAAFRNGHNFMVRN-FRCGQPLQ,[9] which potentially use protein import machinery (e.g., the TOM/TIM complex), have long amino acid sequences and have primarily been used to carry therapeutic proteins (e.g., phospholipase A ortholog (AoPlaA),[8] alanine aminotransferase,[6] tumor suppressor p53,[9] and dihydrofolate reductase.[10] In addition, $(\text{cyclohexyl alanine-arginine})_n$ (n = 3–6) was recently investigated for the delivery of doxorubicin and chlorambucil as a small chemical drug after preparation of these chemical conjugates.[11] However, in general, peptides are expensive and can cause immunogenicity. Other notable moieties for mitochondria targeting are the lipophilic cations (e.g., dequalinium (DQA) and triphenylphosphonium (TPP)), which have been intensively investigated.[12] Unlike hydrophilic cations such as Na^+, which cannot cross the mitochondrial membrane without physical or chemical aid (e.g., carriers),[13] DQA and TPP are both relatively lipid-soluble and positively-charged and can pass easily through the phospholipid bilayer of the mitochondrion.[12] In particular, the "bola" structure of DQA comprises a hydrophilic block and a hydrophobic block that facilitate the formation of self-assembled nanoaggregates called "DQAsomes," which are 70–700 nm in diameter. DQAsomes accumulate in the mitochondrial matrix due to their high mitochondrial affinity.[14] In addition, TPP has a unique chemical structure in which both lipophilic phenyl groups and cationic phosphonium result in specific mitochondrial accumulation as a result of the membrane potential between TPP and the mitochondrial membrane.[15] Using TPP derivatives, various chemical drugs such as vitamins, ATP, chlorambucil, and coenzyme Q10 have been chemically linked for their mitochondria-targeting delivery.[14b] Additionally, TPP has been chemically linked to water-soluble polymers (e.g., poly(ethyleneimine),[16] *N*-(2-hydroxypropyl) methacrylamide) copolymers[17]) or amphiphilic copolymers (e.g., Pluronic F127,[18] poly(lactide-co-glycolide)-*b*-poly(ethylene glycol) (PLGA-*b*-PEG),[19] miktoarm star-shaped poly(ε-caprolactone) (PCL)-PEG,[20] PEG-phosphatidylethanolamine[21]) for targeting the mitochondrion. However, in these polymers, TPP was used as a mitochondria-targeting moiety without its contribution for forming their self-assembled nanostructures.

In this study, TPP was selected as a mitochondria-targeting moiety, and two TPP molecules were chemically linked with two ends of the biocompatible and biodegradable PCL to form a bola-like amphiphilic TPP-*b*-PCL-*b*-TPP (TPCL) polymer, resulting in the construction of cationic nanoparticles (NPs) (**Figure 1**). Although TPP is known as a lipophilic cation, TPCL polymers were designed to form self-assembled nanostructures themselves because PCL is relatively hydrophobic, and cationic TPP is relatively hydrophilic in the TPCL polymers. Unlike other aforementioned TPP-modified polymers, the TPP in the TPCL polymers was designed to have dual roles as both an essential component for constructing their nanosized self-assemblages and as a mitochondria-targeting moiety. The resulting self-assembled nanostructures could encapsulate therapeutics. Additionally, the positive surface charge of TPCL NPs could damage cell viability, resulting in their role as a "nanodrug" for antitumor therapies. Thus, it is expected that

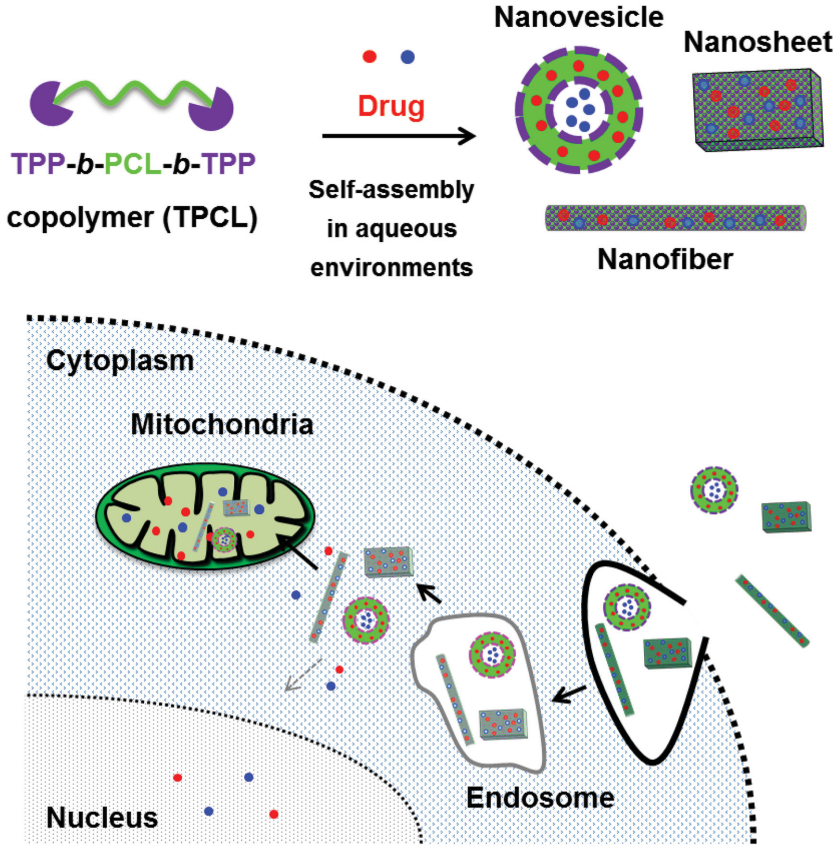

Figure 1. Illustrated design concept of drug-loaded TPCL nanoparticles (NPs) in cells. Red color solid circle (●) and blue color solid circle (●) indicate hydrophobic and hydrophilic chemical drugs, respectively.

TPCL NPs could act as nanosized drugs themselves as well as nanosized drug delivery carriers for mitochondria-targeting delivery of payloads. This study investigated the synthesis and characterization of TPCL polymers and the physicochemical, biological, morphological, and drug-encapsulating characteristics of drug-free or drug-loaded TPCL NPs for specific mitochondria targeting. Specifically, the antitumor effects of TPCL NPs themselves as well as anticancer drug-loaded TPCL NPs were evaluated.

2. Results and Discussion

2.1. Synthesis and Chemical and Physical Characteristics of TPP-*b*-PCL-*b*-TPP (TPCL) Copolymers

To synthesize the designed TPCL copolymers, two hydroxyl groups at two ends of the PCL diol were chemically coupled with two molecules of 4-carboxybutyltriphenylphosphonium bromide (TPP^+–$COOH \cdot Br^-$), which has one carboxylic acid, via a conventional conjugation reaction (**Figure 2**). The chemical structure of the TPCL copolymers was confirmed by assigning notable peaks in the ^{1}H-NMR spectra in $CDCl_3$ (**Figure 3**a). Based on the integration ratio of the associated peak for $(C_6\underline{H}_5)_3$-P^+- in the TPP moiety at δ 7.6–7.9 and the associated peaks for either —C(=O)OCH$_2$C$\underline{H}_2$C$\underline{H}_2$C$\underline{H}_2$C$\underline{H}_2$C(=O)O— or —C(=O)OCH$_2$CH$_2$CH$_2$CH$_2$C$\underline{H}_2$C(=O)O— in the PCL backbone at δ 1.3–1.7 or δ 2.2–2.4, respectively, the molar TPP ratios in the TPCL1 (TPP-$PCL_{1.25\ kDa}$-TPP) and TPCL2 (TPP-$PCL_{2\ kDa}$-TPP) copolymers were 1.8 and 1.9, respectively, as a duplicate average, and the results were converted to estimate the molecular weights (M_{Ws}) of the TPCL1 (1900 Da) and TPCL2 (2690 Da) copolymers.

Neither $PCL_{1.25\ kDa}$ diol nor $PCL_{2\ kDa}$ diol demonstrated any significant absorptions at 200–300 nm, whereas a remarkable absorption peak of the phenyl groups in TPP^+-$COOH \cdot Br^-$ was represented at 267 nm. The presence of TPP in the TPCL copolymers was further confirmed by the unique absorption of TPP in the UV/visible spectra, and the molar TPP ratios in the TPCL1 and TPCL2 copolymers were 1.7 and 2.1, respectively, as a duplicate average (Figure 3b). Using gel permeation chromatography (GPC), the additional M_W analysis demonstrated that the number-average M_{Ws} (M_n) of the TPCL1 and TPCL2 copolymers were 2300 Da (polydispersity (PDI) 1.19) and 3680 Da (PDI 1.29), compared with the M_{Ws} of $PCL_{1.25\ kDa}$ diol and $PCL_{2\ kDa}$ diol, which were 1950 Da (PDI 1.29) and 3110 Da (PDI 1.40), respectively (Figure S1, Supporting Information).

Based on the ^{1}H-NMR spectra, UV/visible spectra, and GPC chromatograms of the TPCL copolymers (Figure 3 and Figure S1, Supporting Information), the polymeric architecture of the synthesized TPCL1 and TPCL2 copolymers was almost a bola form, with the amphiphilic TPP-PCL-TPP copolymers having the relatively hydrophobic PCL and the relatively hydrophilic TPP as designed to mimic the amphiphilic DQA. Thus, it might be expected that the amphiphilic and cationic TPCL copolymers could be self-assembled.

2.2. Physicochemical Characteristics of Self-Assembled TPCL Nanoparticles (NPs)

It is known that various factors (e.g., temperature, polymer-solvent interaction, the presence of additives, preparation methods) influence the physicochemical and morphological characteristics of self-assembled NPs made from amphiphilic polymers.[22] Thus, using the synthesized TPCL copolymers, their self-assembled NPs were prepared in two ways; one was cosolvent dispersion (CD) and the other was film hydration (FH). The resulting TPCL NPs were designated TPCL1-CD NPs, TPCL2-CD NPs, TPCL1-FH NPs, and TPCL2-FH NPs.

The physicochemical characteristics (e.g., particle size and zeta-potentials) of the prepared TPCL NPs were measured to confirm whether they were really NPs (**Table 1** and **Figure 4** and Table S2, Supporting Information). When monitoring their sizes by light scattering (LS) at a fixed angle (90°), the TPCL-CD NPs had a smaller size than the TPCL-FH NPs (Table 1). However, in their morphological evaluation with cryo-transmission electron microscopy (cryo-TEM), the TPCL NPs exhibited different nanostructures depending on the preparation method (Figure 4). The TPCL2-CD NPs were mostly nanofibers that were 8–9 nm in width, with few nanosheets. Although some of the TPCL2-FH NPs were nanofibers approximately 7 nm in width, their major nanostructure was nanovesicles that were 50–200 nm in size with a layer thickness of approximately 7 nm. Interestingly,

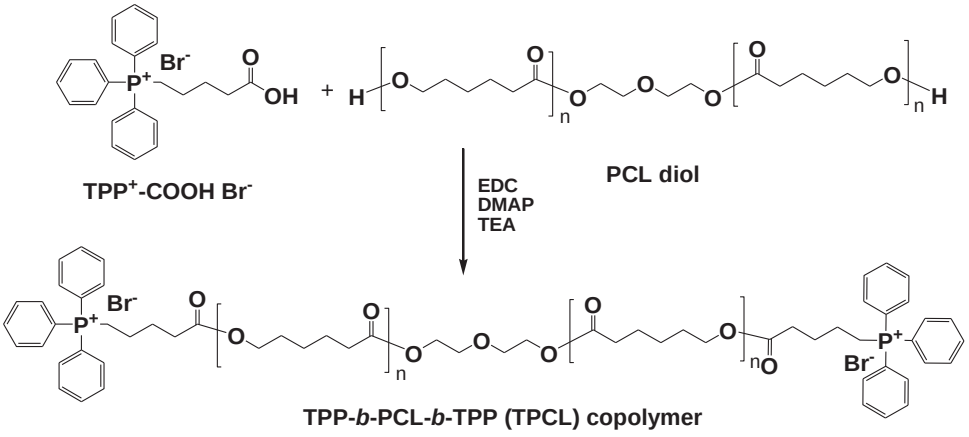

Figure 2. Synthetic scheme of TPP-*b*-PCL-*b*-TPP (TPCL) copolymers.

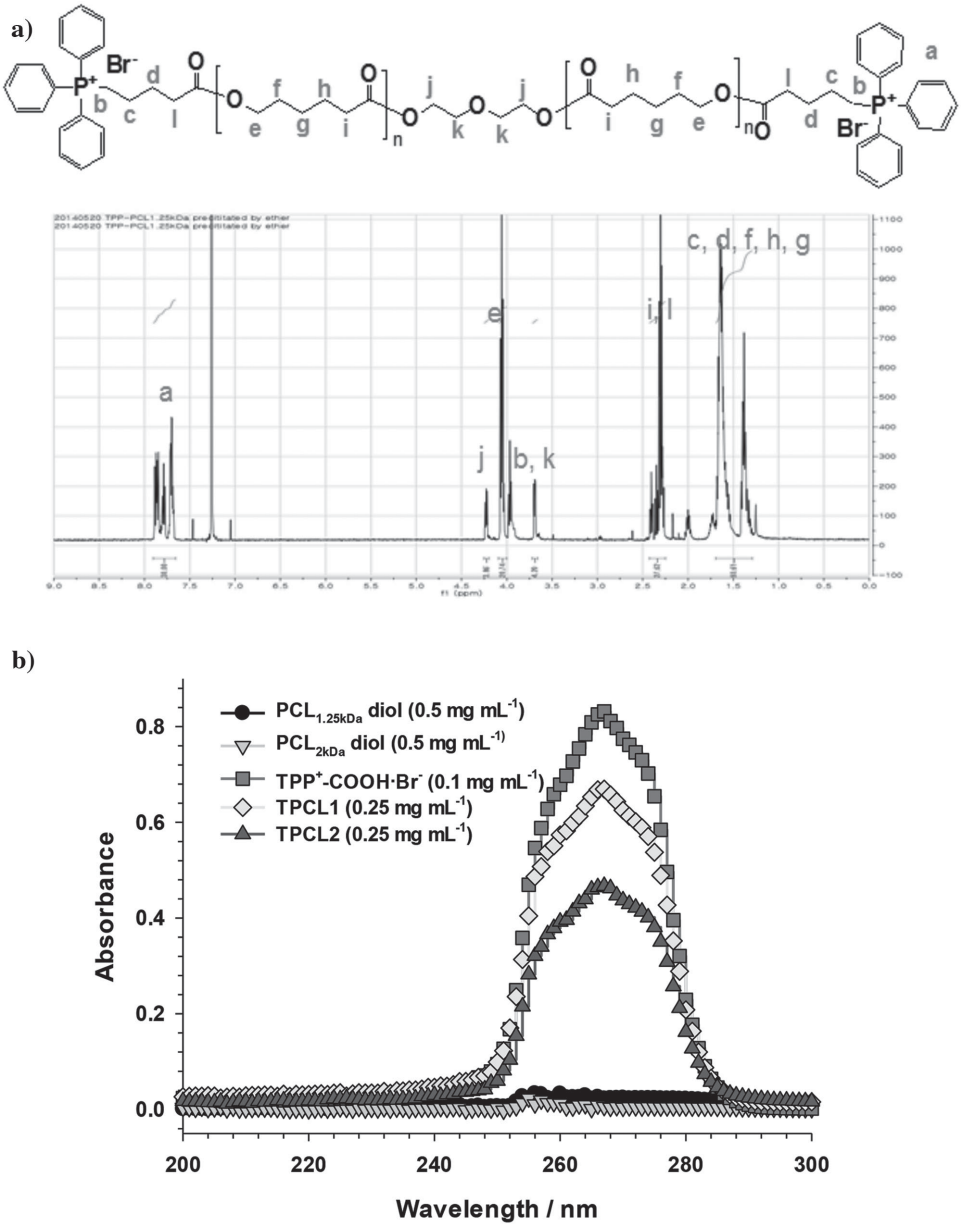

Figure 3. a) ^{1}H-NMR spectra and b) UV/visible spectra of TPCL copolymers.

the sizes of the TPCL NPs were different depending on the LS and cryoTEM method. In particular, the size measurements of the TPCL-CD nanofibers using LS might not be suitable because a fixed-angle LS technique only estimates the sizes of spheres. The reason might cause two different size distributions of mostly 10–20 nm in size and relatively few of 50–200 nm in size when evaluated by LS (Figure S2, Supporting Information). In addition, the estimated volume fraction values for the relatively hydrophilic portion (i.e., TPP) (f_{TPP}) of the TPCL copolymers were approximately 0.25–0.35 based on the densities of the bulk polymers/molecules ($\rho_{TPP} \approx 1.2$ g cm^{-3} and $\rho_{PCL} = 1.25$ g cm^{-3}), and this supported the vesicular structure of the TPCL NPs based on literature results.[23] However, it is unclear why the TPCL NPs also have other nanostructures such as nanofibers and nanosheets.

The zeta-potentials of the TPCL-CD NPs and the TPCL-FH NPs at approximately 40 mV were not significantly different. The positive surface charges of the NPs indicate that some TPP moieties may have been placed on the outside of the NPs. It further suggests that the exterior TPP molecules in the NPs could be used to target the mitochondria and penetrate the mitochondrial membrane.

2.3. Biological Characteristics of Self-Assembled TPCL NPs

Mitochondria-targeting moieties are effective for the delivery of selective therapeutics to the mitochondria. Many well-known mitochondria-targeting moieties have cationic characteristics to

Table 1. Characteristics of drug-free TPCL NPs and drug-loaded TPCL NPs.

NP code name	NP preparation		Drug loading	
	Size [nm][a)]	Zeta-potential [mV]	Efficiency [%]	Content [wt%]
TPCL1-CD NP	12 ± 1.4	45 ± 13	–	–
TPCL2-CD NP	15 ± 4.9	41 ± 10	–	–
TPCL1-FH NP	23 ± 13	37 ± 17	–	–
TPCL2-FH NP	52 ± 32	41 ± 17	–	–
Dox-TPCL1-CD NP	23 ± 12	51 ± 13	42 ± 1	9.5 ± 0.3
Dox-TPCL2-CD NP	32 ± 14	71 ± 17	39 ± 4	8.9 ± 0.8
Dox-TPCL1-FH NP	76 ± 41	41 ± 8	7.6 ± 5	1.8 ± 1.0
Dox-TPCL1-FH NP	45 ± 12	35 ± 13	15 ± 4	3.6 ± 1.0
Dox·HCl-TPCL1-CD NP	61 ± 17	26 ± 2	15± 3	3.5 ± 0.6
Dox·HCl-TPCL2-CD NP	31 ± 23	29 ± 10	19 ± 11	4.5 ± 3.0
Dox·HCl-TPCL1-FH NP	18 ± 10	20 ± 3	20 ± 13	4.9 ± 3.0
Dox·HCl-TPCL2-FH NP	43 ± 26	19 ± 2	16 ± 6	3.8 ± 1.4

[a)]Particle size was measured by light scattering at a fixed angle (90°). Data are expressed as the mean ± standard deviation ($n = 3$).

aid therapeutics and drug-delivery systems in penetrating the mitochondrial membrane due to differences in the membrane potentials.[15] However, their cationic nature could induce some mitochondrial damage and, ultimately, cell death. The antitumor effects of TPP salts were investigated,[24] and TPP-conjugated polyethyleneimine (PEI) also exhibited dose-dependent cytotoxicity.[16] Recently, although stearyl TPP (STPP)-containing liposomes did not encapsulate anticancer chemicals, the liposomes exhibited cytotoxicity against tumor cells, and in particular, greater STPP content in the liposomes resulted in greater antitumor effects.[25] Additionally, mitochondria-targeting $(\text{cyclohexylalanine-arginine})_n$ peptides with higher numbers of the repeating unit (e.g., $n = 4$–6) caused much more cytotoxicity than those with lower repeating unit numbers (e.g., $n = 3$).[11a]

Thus, there was concern about the cytotoxicity of the designed TPCL NPs because the NPs had positively charged surfaces regardless of their preparation method (Table 1). As shown in **Figure 5**, a relatively hydrophilic TPP derivative (i.e., 4-(carboxylbutyl)TPP·Br (TPP^+-$COOH \cdot Br^-$) used in this study did not demonstrate an IC_{50} (the drug concentration that causes 50% growth inhibition) values at the concentrations tested (i.e., ≤0.4 mg mL^{-1}), whereas a hydrophobic TPP derivative (i.e., methoxymethyl TPP·Cl) had IC_{50} values of approximately 0.2 mg mL^{-1} in HeLa and HepG2 cells. However, when administering TPCL NPs to HeLa cells for 48 h, their IC_{50} values were approximately 42 μg mL^{-1} for TPCL1-CD NPs, approximately 24 μg mL^{-1} for TPCL2-CD NPs, approximately 30 μg mL^{-1} for TPCL1-FH NPs, and approximately 12 μg mL^{-1} for TPCL2-FH NPs (Figure 5a). Similarly, 48 h treatment of HepG2 cells with TPCL1-CD NPs, TPCL2-CD NPs, TPCL1-FH NPs, and TPCL2-FH NPs resulted in IC_{50} values of approximately 58 μg mL^{-1}, 39 μg mL^{-1}, 51 μg mL^{-1}, and 13 μg mL^{-1}, respectively (Figure 5b). Despite the similar zeta-potentials of the TPCL NPs, their cytotoxic results indicate that the TPCL2-based NPs were approximately 1.5–3.9-fold more cytotoxic than the TPCL1-based NPs and that the FH method resulted in approximately 1.1–3-fold more cytotoxic TPCL NPs than the CD method. In addition, the TPCL-CD NPs and TPCL-FH NPs exhibited approximately 3–8-fold and 4–17-fold better antitumor effects than methoxymethyl TPP·Cl. Thus, our findings suggest that TPCL NPs themselves can play a role as a nano-sized drug to kill tumor cells.

2.4. Physicochemical Characteristics and Drug Release of Drug-Loaded TPCL NPs

Although the cytotoxic results with TPCL NPs (Figure 5) suggest their potential as an anticancer nanodrug, the self-assembled TPCL NPs could play a role as a drug delivery carrier due to their ability to encapsulate therapeutics. Additionally, in general, self-assembled nanoparticles load either hydrophobic drugs or hydrophilic drugs. Most nanoparticles (e.g., micelles) load hydrophobic doxorubicin free base (Dox) instead of hydrophilic doxorubicin hydrochloride (Dox·HCl) because the hydrophobic drug can be encapsulated well for high drug loading contents. Thus, we evaluated whether the TPCL NPs could be loaded with either a hydrophilic chemical or a hydrophobic chemical depending on the NP preparation method (i.e., CD or FH). First, the drug-loading efficiency (DLE,%) and drug-loading content (DLC, wt%) of drug-loaded TPCL NPs were assessed because a high DLE could reduce the loss of drug and a high DLC could reduce the required amounts of NP components. When loading Dox as a hydrophobic

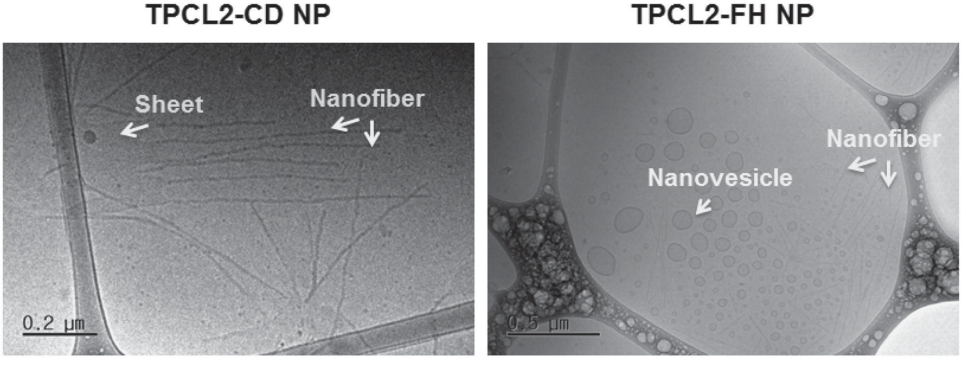

Figure 4. CryoTEM images of drug-free TPCL NPs.

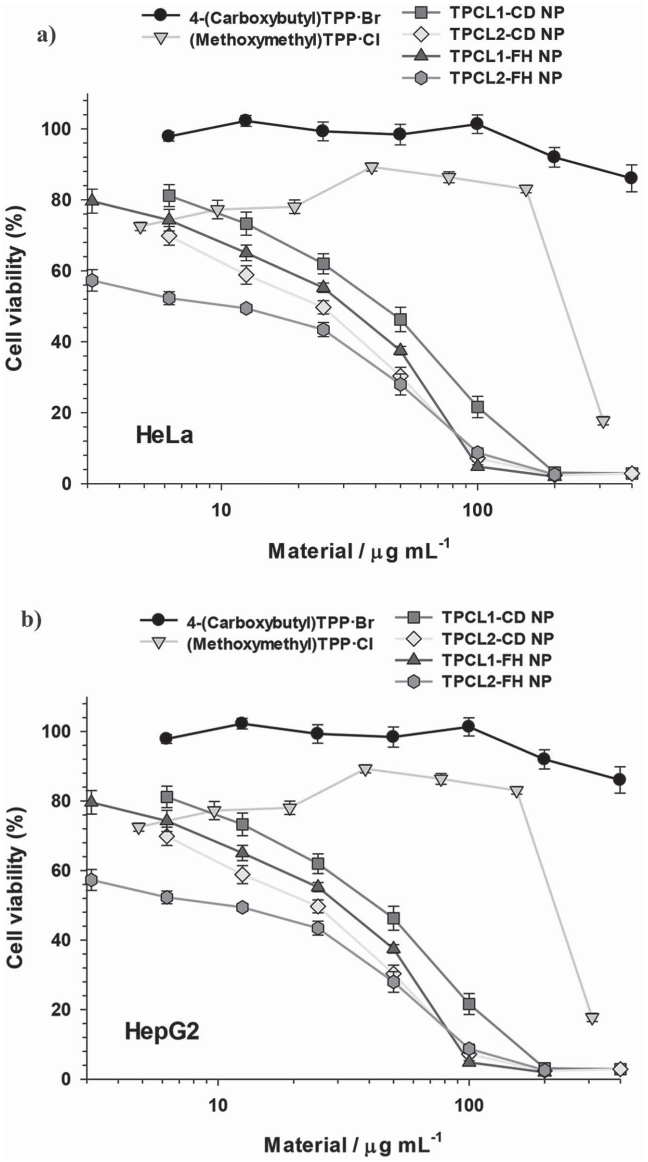

Figure 5. In vitro cytotoxicity of TPP derivatives and drug-free TPCL NPs in a) HeLa and b) HepG2 cells at 48 h post-treatment. The TPP derivatives and drug-free TPCL NPs at various concentrations were administered to the cells for 48 h, and the data were expressed as the mean ± standard error (n = 12–30).

therapeutic into TPCL NPs during NP preparation, the Dox-TPCL-CD NPs had approximately 2.5–5.3-fold higher DLE and DLC than the Dox-TPCL-FH NPs (Table 1). However, after making TPCL NPs using either CD or FH, the loading of a hydrophilic Dox·HCl resulted in a similar DLE (average 15%–20%) and DLC (average 3.5–5 wt%), regardless of the NP preparation method. Although both the hydrophilicity/hydrophobicity and loading methods of a drug strongly affect its loading content in TPCL NPs, these findings indicate that different nanostructured TPCL NPs having either nanovesicles or nanofibers can encapsulate both hydrophilic and hydrophobic chemical drugs (e.g., Dox·HCl and Dox).

For their size and surface charge, the Dox-loaded TPCL NPs exhibited somewhat larger particles with similar or slightly higher positive surface charges than drug-free TPCL NPs (Table 1). In particular, the Dox-TPCL-FH NPs had larger sizes and less positive zeta-potentials than the Dox-TPCL-CD NPs. In the case of Dox·HCl, the Dox·HCl-loaded TPCL NPs had a size of 20–60 nm and zeta-potentials of 20–30 mV. In particular, the Dox·HCl-TPCL-FH NPs demonstrated less positive zeta-potentials than the Dox·HCl-TPCL-CD NPs compared with the zeta-potentials of the Dox-TPCL NPs. The results indicate that the loading methods and the hydrophobicity/hydrophilicity of drugs affect the changes in the sizes and surface charges of drug-loaded TPCL NPs compared with drug-free TPCL NPs.

To measure drug release from drug-loaded TPCL NPs in deionized water (DIW) at 37 °C, two different methods were used. For Dox·HCl-loaded TPCL NPs, the NPs were added into a dialysis device, and then the permeated Dox·HCl was monitored. However, for the Dox-loaded TPCL NPs, the dialysis device was not applied because the released Dox would not be soluble in water and the Dox would rarely permeate through the device membrane. Thus, instead of hydrophobic Dox, a hydrophobic Nile red (NR) was used because the fluorescence of the NR is emitted in hydrophobic environments (e.g., the hydrophobic compartment of NPs) but is quenched in polar environments (e.g., water).[26] In the dialysis device, the Dox·HCl was completely permeated within 6 h, whereas the Dox·HCl released from the Dox·HCl-loaded TPCL NPs was approximately fivefold slower to fully permeate (**Figure 6**a). Particularly, although the release of Dox·HCl was not significantly affected by the NP preparations, the Dox·HCl-TPCL1 NPs exhibited slightly faster Dox·HCl release than the Dox·HCl-TPCL2 NPs. These findings might be caused by the fact that the TPCL2 had a longer hydrophobic PCL block length than the TPCL1. In the case of the NR-loaded TPCL NPs, the NR release was very slow, and the released NR (%) was below 10% for 6 h (Figure 6b). The NR-TPCL1 NPs exhibited slightly faster NR release than the NR-TPCL2 NPs. Interestingly, faster NR release from the NR-TPCL-CD NPs was observed compared with the NR release from the NR-TPCL-FH NPs. It could be caused by different surface areas per unit mass because nanofibers have higher specific surface area than nanovesicles.

2.5. In Vitro Antitumor Characteristics of Drug-Loaded TPCL NPs

The TPCL NPs exhibited antitumor effects as nanodrugs (Figure 5) and encapsulated both hydrophobic Dox and hydrophilic Dox·HCl (Table 1). Additionally, although Dox and Dox·HCl are frequently loaded into nanocarriers, it is difficult to find comparisons of their antitumor effects. Thus, to describe whether the TPCL NPs efficiently deliver therapeutics to cells and which drug is more effective between Dox and Dox·HCl, the delivery efficiency of the drug-loaded TPCL NPs was evaluated and compared with free drugs in an MTT-based cell viability assay (**Figure 7** and **Table 2**). In HeLa and HepG2 cells, the IC_{50} values of free Dox·HCl were approximately 3.5-fold lower than free Dox, indicating that the hydrophilic drug was a more potent anticancer drug than the hydrophobic drug. In HeLa cells, Dox-loaded TPCL NPs and Dox·HCl-loaded TPCL NPs exhibited 1.4–7.3-fold and 4.3–18.6-fold higher antitumor

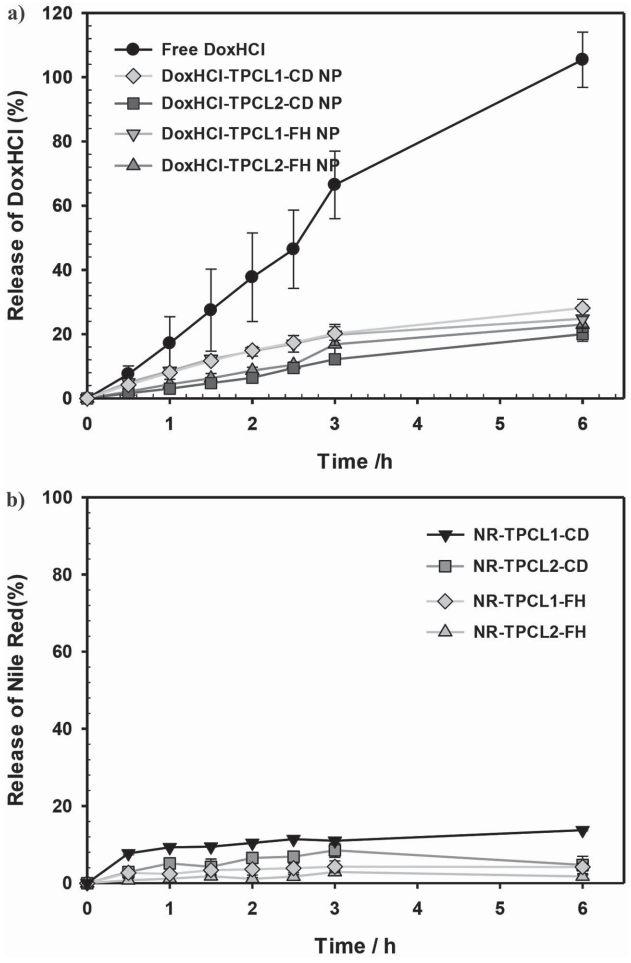

Figure 6. Time-dependent drug release of drug-loaded TPCL NPs: a) Dox·HCl-TPCL NPs and b) NR-TPCL NPs in DIW at 37 °C. The data were expressed as the mean ± standard deviation ($n = 3$).

effects than free Dox and free Dox·HCl, respectively, as demonstrated by their lower IC_{50} values (Figure 7a,b). With the exception of the IC_{50} values of the Dox-TPCL1-FH NPs (3.2 μg mL^{-1}) and the Dox·HCl-TPCL1-CD NPs (0.6 μg mL^{-1}), the other Dox-loaded TPCL NPs and the Dox·HCl-loaded TPCL NPs demonstrated 1.4–2.6-fold and 2–7.5-fold higher tumor-killing activity than free Dox and free Dox·HCl, respectively (Figure 7c,d).

Similarly, for TPCL-CD NPs, the Dox·HCl-loaded NPs had 4.7–10-fold (for HeLa) and 2.8–3-fold (for HepG2) superior cell-killing activity compared with the Dox-loaded NPs, and for TPCL-FH NPs, the Dox·HCl-loaded NPs demonstrated 8.6–45.7-fold (for HeLa) and 13.8–40-fold (for HepG2) higher antitumor effects than the Dox-loaded NPs. The results might be influenced by higher aqueous solubility and faster release of Dox·HCl than Dox. However, interestingly, the antitumor effects of the drug-loaded TPCL NPs might have been slightly influenced by the NP preparation methods. The Dox-TPCL-CD NPs exhibited similar or up to 2.3-fold superior drug efficacy compared with the Dox-TPCL-FH NPs, whereas the Dox·HCl-TPCL-FH NPs had 1.4–7.5-fold better antitumor potency than the Dox·HCl-TPCL-CD NPs. Additionally, when applying the same loaded drugs and NP preparation methods, the drug-loaded TPCL2 NPs had similar or up to 5.3-fold better killing effects than the drug-loaded TPCL1 NPs. In particular, although the drug-free TPCL NPs exhibited much lower antitumor effects (i.e., 2.7–9.5-fold and 9.2–32-fold lower in HeLa cells and 5.7–25.2-fold and 21.6–96.7-fold lower in HepG2 cells) than free Dox and free Dox·HCl, respectively, the Dox-loaded TPCL NPs and the Dox·HCl-loaded TPCL NPs demonstrated 9.4–30-fold and 140–428-fold, respectively, better killing effects in HeLa cells and 11.8–43.3-fold and 96.7–638-fold, respectively, better antitumor effects in HepG2 cells than drug-free TPCL NPs. These results indicate that the simultaneous delivery of TPCL NPs and chemical drugs in a single nanocarrier could induce synergistic antitumor effects compared with single delivery of either free drugs or TPCL NPs themselves because the IC_{50} values of the free drugs (Figure 7 and Table 2) and the TPCL NPs (Figure 5) were much higher than the drug-loaded TPCL NPs.

2.6. Intracellular Distributions, Cellular Uptake, Nuclear Uptake, and Mitochondrial Uptake of Drug-Loaded TPCL NPs

Compared with the antitumor effects of free drugs and the drug-free TPCL NPs, the synergistically higher antitumor results of the drug-loaded TPCL NPs might not be attributable solely to the simple combination of the antitumor effects of the loaded drugs and the cell-killing activity of the TPCL NPs themselves. Thus, the cellular uptake and intracellular distribution of the chemical drugs delivered by the TPCL NPs were further analyzed because drug- or NP-mediated antitumor effects are strongly affected by their cellular uptake, which is also controlled by various factors such as size,[27] zeta-potential,[28] hydrophilicity/hydrophobicity,[29] and morphology.[30]

First, the intracellular distribution of the drug-loaded TPCL NPs was monitored by confocal microscopy because both the intracellular intensity and location of the Dox (or Dox·HCl) fluorescence could strongly influence the antitumor effects of Dox (or Dox·HCl). The nucleus and the mitochondria were stained with Hoechst33342 (encoded as a blue color) and MitoTracker (encoded as a red color), respectively, to estimate the intracellular locations of the drugs delivered with or without drug-loaded NPs (encoded with a green color). Additionally, for this study, the Dox-TPCL-CD NPs and Dox·HCl-TPCL-FH NPs were selected as model drug-loaded TPCL NPs because these NPs exhibited better antitumor effects than the Dox-TPCL-FH NPs and Dox·HCl-TPCL-CD NPs. When applying either free drug or drug-loaded TPCL NPs with [Dox] = 1 μg mL^{-1} to HeLa cells (3×10^4 cells in 0.3 mL), the intracellular fluorescence intensity of the free Dox·HCl was much stronger than the Dox-TPCL1-CD NPs or the Dox-TPCL2-CD NPs and was similar to the Dox·HCl-TPCL1-FH NPs (**Figure 8**a). However, the Dox·HCl-TPCL2-FH that had been taken up as NPs in HeLa cells demonstrated higher intracellular fluorescence than in the free Dox·HCl-treated cells. The confocal results indicate that the cellular uptake of the free drugs and drug-loaded NPs could be arranged in the following order: Dox·HCl-TPCL2-FH NPs >> Dox·HCl-TPCL1-FH NPs ≈ free Dox·HCl >> Dox-TPCL1-CD NPs ≈ Dox-TPCL2-CD NPs. In particular, when overlapping the fluorescence of the free drugs with the stained

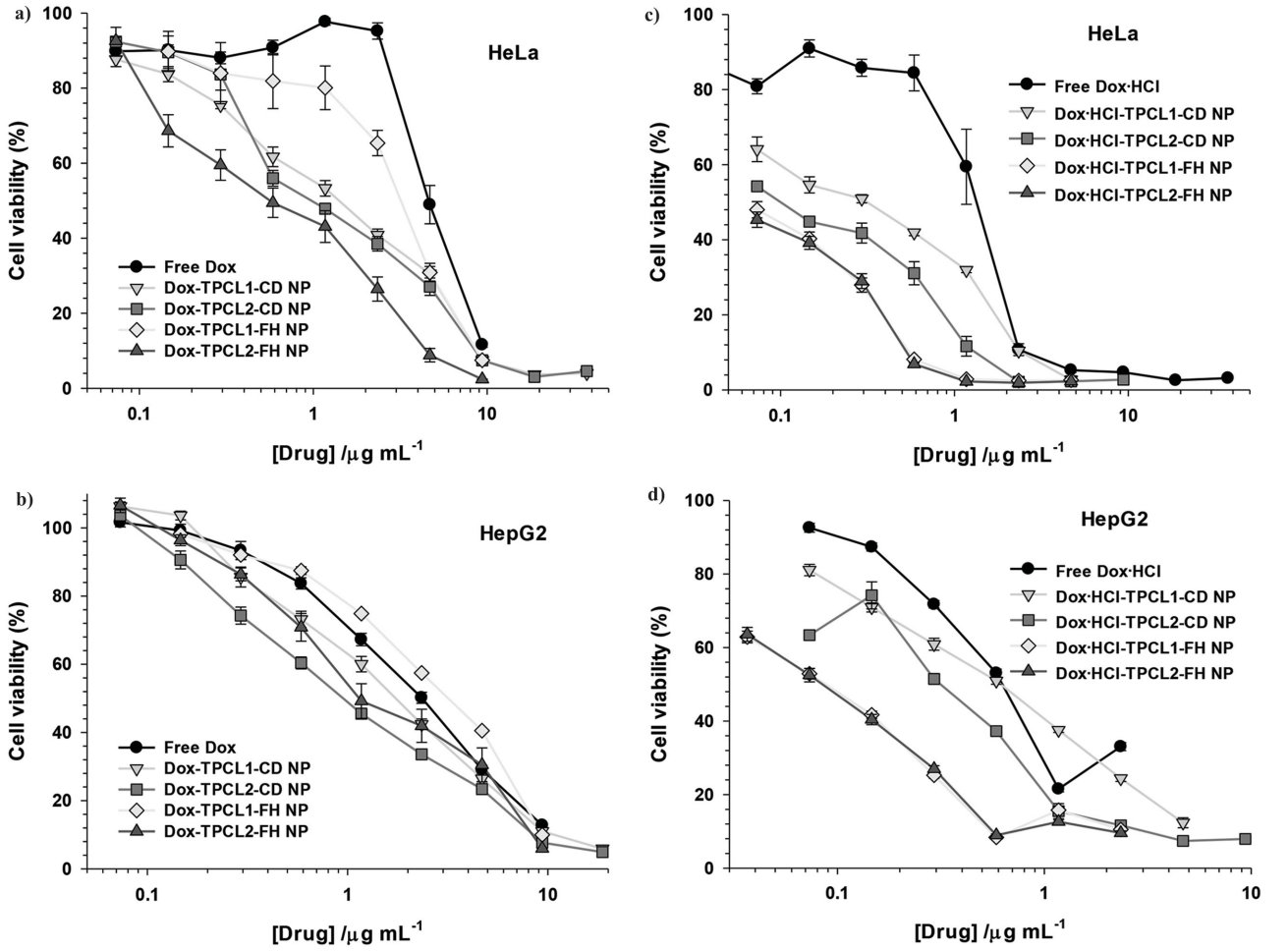

Figure 7. In vitro antitumor effects of a) Dox-loaded TPCL NPs and b) Dox·HCl-loaded TPCL NPs in HeLa cells and c) Dox-loaded TPCL NPs and d) Dox·HCl-loaded TPCL NPs in HepG2 cells at 48 h post-treatment. The drug-loaded NPs and free drugs at various concentrations were administered to the cells for 48 h, and the data were expressed as the mean ± standard error (n = 24–30).

Table 2. Antitumor effects (IC_{50}) and normalized cellular uptake (CU), nuclear uptake (NU), and mitochondrial uptake (MU) of free drugs and drug-loaded TPCL NPs in HeLa and HepG2 cells. (For the CU, NU, and MU of the drug-loaded TPCL NPs, the NPs with [Dox] = 5 μg mL^{-1} were incubated with cells for 4 h, and the data were expressed as the mean ± standard error (n = 3). The antitumor effects of the drug-loaded TPCL NPs were evaluated at 48 h post-treatment after treatment with the NPs having different drug concentrations.)

	HeLa cells				HepG2 cells			
	IC_{50} [μg mL^{-1}]	Normalized CU	Normalized NU	Normalized MU	IC_{50} [μg mL^{-1}]	Normalized CU	Normalized NU	Normalized MU
Dox	4.4	0.33 ± 0.03	0.37 ± 0.06	0.93 ± 0.23	2.3	0.47 ± 0.04	0.34 ± 0.05	0.68 ± 0.07
Dox-TPCL1-CD NP	1.4	0.24 ± 0.02	0.23 ± 0.03	1.69 ± 0.59	1.7	0.31 ± 0.06	0.27 ± 0.05	0.64 ± 0.12
Dox-TPCL2-CD NP	1.0	0.22 ± 0.01	0.21 ± 0.03	1.45 ± 0.39	0.9	0.30 ± 0.03	0.21 ± 0.03	0.52 ± 0.10
Dox-TPCL1-FH NP	3.2	0.23 ± 0.04	0.35 ± 0.11	1.58 ± 0.71	3.2	0.64 ± 0.25	0.63 ± 0.24	1.78 ± 0.97
Dox-TPCL2-FH NP	0.6	0.18 ± 0.04	0.29 ± 0.07	1.16 ± 0.41	1.1	0.37 ± 0.06	0.36 ± 0.11	0.62 ± 0.17
Dox·HCl	1.3	1	1	1	0.6	1	1	1
Dox·HCl-TPCL1-CD NP	0.3	0.55 ± 0.11	0.71 ± 0.19	3.77 ± 1.78	0.6	0.98 ± 0.26	0.97 ± 0.31	1.47 ± 0.28
Dox·HCl-TPCL2-CD NP	0.1	0.53 ± 0.16	0.85 ± 0.26	3.54 ± 1.35	0.3	0.94 ± 0.21	1.12 ± 0.35	1.68 ± 0.40
Dox·HCl-TPCL1-FH NP	< 0.07	0.96 ± 0.26	0.87 ± 0.17	3.40 ± 1.33	0.09	1.35 ± 0.32	1.25 ± 0.31	2.17 ± 0.57
Dox·HCl-TPCL2-FH NP	< 0.07	1.30 ± 0.38	1.20 ± 0.23	2.43 ± 0.49	0.09	1.61 ± 0.42	1.38 ± 0.39	1.99 ± 0.46

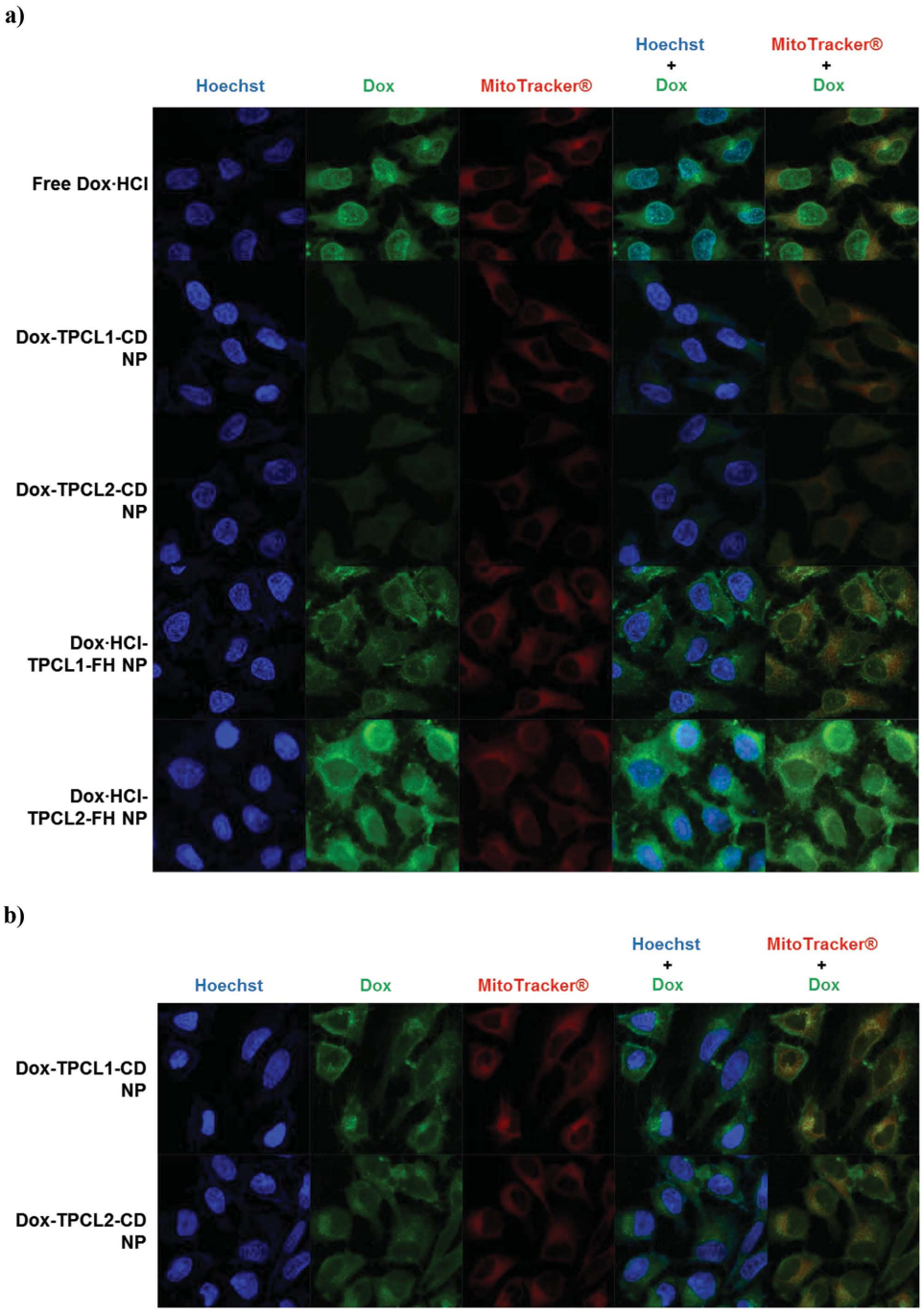

Figure 8. Intracellular distribution of a) free drugs and drug-loaded TPCL NPs and b) Dox-TPCL-CD NPs with [Dox] = 1 μg mL^{-1} in HeLa cells at 4 h post-treatment. Increased laser intensity for b) experiments was used.

subcellular organelles (i.e., the nucleus and the mitochondria), the majority of the free Dox·HCl was localized in the nucleus, while a minor portion was detected in the mitochondria. However, interestingly, it seems that the Dox·HCl-TPCL1-FH NPs and the Dox·HCl-TPCL2-FH NPs were much more localized in the mitochondria than in the nucleus. For the Dox-TPCL1-CD NPs and the Dox-TPCL2-CD NPs, their intracellular distribution in Figure 8a was unclear due to their very low fluorescence intensities at [Dox] = 1 μg mL^{-1}. On increasing the laser intensity to detect the drug fluorescence, it was found that the intracellular localization of the Dox-TPCL1-CD NPs and Dox-TPCL2-CD NPs occurred mostly in the mitochondria but not in the nucleus (Figure 8b). These confocal images indicated that drug-loaded TPCL NPs accumulated much more in the mitochondria than in the nucleus, unlike the free Dox·HCl.

In addition, the cellular uptake of the free drugs and the drug-loaded TPCL NPs was further evaluated by flow cytometry after either free drugs or drug-loaded NPs at [drug] = 5 μg mL^{-1} were

used to treat the cells (5×10^5 cells in 2 mL) for 4 h. The fluorescence intensities of the free Dox·HCl in HeLa and HepG2 cells were approximately 3-fold and 2.1-fold higher than free Dox, respectively (Table 2, and Figures S3 and S4, Supporting Infromation). Most of the Dox-loaded TPCL NPs had 1.4–1.9-fold (in HeLa) and 1.3–1.6-fold (in HepG2) lower fluorescence intensities than free Dox, indicating that the drug-delivery efficiency of the Dox-loaded TPCL NPs was approximately 53%–77% of the drug-delivery efficiency of free Dox. Additionally, except for the cellular uptake of the Dox·HCl-TPCL-CD NPs in HeLa cells, the other Dox·HCl-loaded TPCL NPs exhibited similar or slightly greater (0.95–1.5-fold) cellular uptake than free Dox·HCl in HeLa and HepG2 cells. The flow cytometry results for the cellular uptake of the drug-loaded NPs supported their intracellular intensity results as determined by confocal microscopy (Figure 8a). However, the lower cellular uptake of the Dox-loaded TPCL NPs compared with the free Dox and the similar or slightly better cellular uptake of the Dox·HCl-loaded TPCL NPs compared with the free Dox·HCl did not clearly explain why the drug-loaded TPCL NPs had much higher antitumor effects than the free drugs.

We further focused on the nuclear and mitochondrial distribution of the free drugs and the drug-loaded TPCL NPs because they are important subcellular organelles for cell proliferation and cell death. Additionally, although the confocal microscopy results described greater mitochondrial localization of the drug-loaded TPCL NPs than the free drugs, it was still difficult to determine whether the drug-loaded TPCL NPs really existed in the mitochondria or the cytoplasm because the mitochondria are spread throughout the whole cytoplasm. Thus, after isolating the nuclei and the mitochondria from cells prepared for cellular uptake studies of drug-loaded TPCL NPs, the intracellular localization and intensity of the free drugs and the drug-loaded NPs were further confirmed by flow cytometry. As shown in Table 2 and Figures S3 and S4, Supporting Infromation, the nuclear uptake of the free drugs and the drug-loaded TPCL NPs exhibited similar trends in their cellular uptakes, whereas interestingly, the mitochondrial uptake of the drug-loaded TPCL NPs was similar or higher than of the free drugs. In HeLa and HepG2 cells, the mitochondrial uptake of free Dox was approximately 93% and 68% of the mitochondrial uptake of free Dox·HCl, respectively. The Dox-loaded TPCL NPs were approximately 1.3–1.8-fold (in HeLa cells) and 0.8–2.6-fold (in HepG2 cells) more localized in the mitochondria than free Dox. Additionally, the Dox·HCl-loaded TPCL NPs were approximately 2.4–3.8-fold (in HeLa cells) and 1.5–2.2-fold (in HepG2 cells) more localized in the mitochondria than free Dox·HCl.

In particular, when calculating the mitochondria-to-nucleus preference (MNP), the hydrophobic Dox interestingly exhibited preferred accumulation in the mitochondria over the nucleus, and its MNP was 2.5-fold and 2.0-fold higher than free Dox·HCl in HeLa and HepG2 cells, respectively (**Figure 9**). The Dox-loaded TPCL NPs represented 1.6–2.9-fold (in HeLa) and 0.9–1.4-fold (in HepG2) higher MNPs than free Dox, whereas the Dox·HCl-loaded TPCL NPs represented 2–5.3-fold (in HeLa) and 1.4–1.7-fold (in HepG2) higher MNPs than free Dox·HCl.

In this study, a well-known mitochondria-targeting moiety, TPP, was chemically linked at both ends of a PCL diol, and then a bola structure was synthesized with TPCL copolymers.

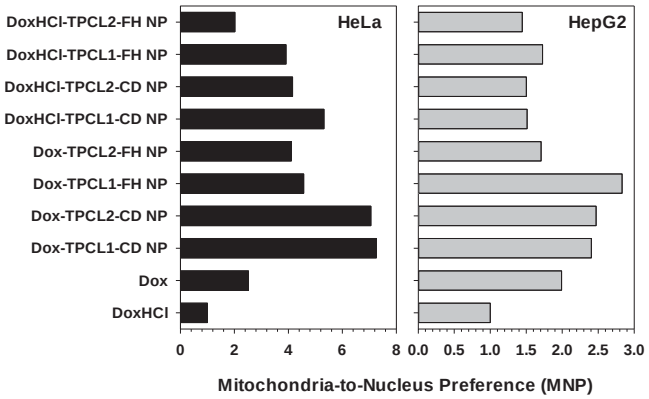

Figure 9. MNP of drug-loaded TPCL NPs in HeLa and HepG2 cells at 4 h post-treatment. The drug-loaded NPs and free drugs (at a fixed concentration of 5 μg mL^{-1}) were administered to the cells for 4 h.

The copolymers formed self-assembled NPs via two different NP preparation methods, specifically CD and FH. Interestingly, the CD and FH methods affected the particles morphologies and resulted in mostly nanofibers and nanovesicles, respectively. Additionally, although the two NP preparation methods did not significantly affect the zeta-potentials of the NPs, CD resulted in smaller TPCL NPs than FH. On in vitro cytotoxicity tests, drug-free TPCL-FH NPs, and TPCL2 NPs exhibited better antitumor effects than drug-free TPCL-CD NPs and TPCL1 NPs, respectively. The antitumor effects of TPCL NPs might be influenced by their sizes and morphologies but not their zeta-potentials.

When encapsulating either hydrophilic Dox·HCl or hydrophobic Dox in TPCL NPs, their loading efficiencies were affected by the drug loading during NP preparation but not the M_w of the PCL block in the TPCL. The loading of Dox during the preparation of the Dox-TPCL-CD NPs and the Dox-TPCL-FH NPs indicated that the former NPs exhibited better drug loading than the latter NPs, whereas the loading of Dox·HCl into the premade TPCL-CD NPs and TPCL-FH NPs did not affect its drug loading. The size and zeta-potentials of the resulting Dox·HCl-TPCL NPs did not show a significant difference depending on the NP preparation method, whereas the Dox-TPCL-CD NPs had slightly smaller sizes and higher positive zeta-potentials than the Dox-TPCL-FH NPs. Although the hydrophilic Dox·HCl represented a much higher cellular uptake and nuclear uptake than the hydrophobic Dox, the slightly higher or similar mitochondrial uptake of Dox·HCl compared with Dox resulted in a lower mitochondrial preference over the nucleus for Dox·HCl compared with Dox. Most of the Dox-TPCL NPs had lower cellular and nuclear uptake but higher mitochondrial preference over the nucleus than Dox, and the Dox·HCl-TPCL NPs presented similar or higher cellular, nuclear, and mitochondrial uptake as well as MNP than free Dox·HCl. The intracellular localization of the free drugs and the drug-loaded TPCL NPs resulted in the drug-loaded TPCL NPs killing similar or greater numbers of tumor cells than the free drugs. In addition, the Dox-TPCL-CD NPs exhibited a lower nuclear uptake and a higher MNP for the nucleus than the Dox-TPCL-FH NPs, leading to higher antitumor effects for the former compared with the latter NPs. Most of the

Dox·HCl-TPCL-FH NPs demonstrated a higher cellular and nuclear uptake but a similar or slightly higher mitochondrial uptake and MNP than the Dox·HCl-TPCL-CD NPs, resulting in higher antitumor effects for the Dox·HCl-TPCL-FH NPs than the Dox·HCl-TPCL-CD NPs.

Based on our findings, the superior antitumor effects of the drug-loaded TPCL NPs compared with their corresponding free drugs may be caused by a combination of cellular uptake, nuclear uptake, and mitochondrial uptake based on the zeta-potentials and sizes of the drug-loaded TPCL NPs as well as the hydrophobicity/hydrophilicity and aqueous solubility of the drugs employed. However, among the possible factors contributing to the antitumor effects, the intracellular localization and MNP of the drug-loaded TPCL NPs could be major factors.

3. Conclusion

In this study, amphiphilic TPP-PCL-TPP (TPCL) polymers were designed and synthesized for the mitochondria-targeting delivery of therapeutics. In aqueous medium, the spontaneous self-assembly of TPCL formed cationic nanoparticles. The TPCL NPs as nanodrugs had potential antitumor effects and encapsulated both hydrophilic and hydrophobic therapeutics. Most of the drug-loaded TPCL NPs exhibited superior tumor-killing activity compared with free drugs, and their preferred accumulation occurred in the mitochondria over the nucleus. In conclusion, such TPCL-based mitochondria-targeting nanoparticles could exert synergistic effects as antitumor therapies due to the dual functionalities of both the nanodrugs themselves and nanocarriers for therapeutics. In addition, TPCL NPs could have potential uses areas such as nanomedicine, subcellular-targeting drug carriers, cell engineering, stem cells or theragnosis.

4. Experimental Section

Materials: Polycaprolactone diols with a M_w of 1.25 kDa ($PCL_{1.25\ kDa}$ diol) and a M_w of 2 kDa ($PCL_{2\ kDa}$ diol) were purchased from Polysciences, Inc. (Warrington, PA, USA) and Sigma-Aldrich Company (St. Louis, MO, USA), respectively. 4-carboxybutyltriphenylphosphonium bromide (TPP^+-$COOH{\cdot}Br^-$), methoxymethyl triphenylphosphonium chloride, 1-ethyl-3-(3-dimethylaminopropyl)carbodiimide (EDC), 4-(dimethylamino) pyridine (DMAP), triethylamine (TEA), chloroform, dimethyl sulfoxide (DMSO), n-hexane, diethyl ether, $CDCl_3$, ammonium sulfate (AS), RPMI-1640 medium, Dulbecco's Modified Eagle's Medium (DMEM), sodium bicarbonate, D-glucose, Ca^{2+}-free and Mg^{2+}-free Dulbecco's phosphate buffered saline (DPBS), 4-(2-hydroxy-ethyl)-1-piperazine (HEPES), fetal bovine serum (FBS), penicillin-streptomycin antibiotics, trypsin-EDTA, 3-(4,5-dimethylthiazol-2-yl)-2,5-diphenyltetrazolium bromide (MTT), Hoechst33342, Nile red (NR), and a Nuclei PURE Prep nuclei isolation kit were purchased from Sigma-Aldrich Company (St. Louis, MO, USA). Doxorubicin hydrochloride (Dox·HCl) and a mitochondria isolation kit were received from MedKoo Biosciences (Chapel Hill, NC, USA) and BioVision (Milpitas, CA, USA), respectively. MitoTracker Deep Red FM was bought from Life Technologies (Grand Island, NY, USA).

Synthesis and Characterization of TPP-PCL-TPP (TPCL) Polymers: TPCL polymers were synthesized via a conventional coupling reaction between a PCL diol and the carboxylic acid of TPP^+–$COOH{\cdot}Br^-$ (Figure 2). In brief, the PCL diol (0.2 g) was dissolved in chloroform (2 mL) and a mixture of TPP^+–$COOH{\cdot}Br^-$ (six equivalent moles of $PCL_{1.25\ kDa}$ diol and $PCL_{2\ kDa}$ diol), EDC (one equivalent mole of TPP^+–$COOH{\cdot}Br^-$), and DMAP (one equivalent mole of TPP^+–$COOH{\cdot}Br^-$) was dissolved in chloroform (8 mL). TEA (0.2 mL) was added into the TPP^+–$COOH{\cdot}Br^-$-containing reaction mixture and then stirred for 2 h to activate the carboxylic acid of TPP^+–$COOH{\cdot}Br^-$. The PCL diol (0.2 g) solution was added into the activated reaction mixture and then was stirred for 2 d under inert nitrogen gas. The resulting reaction solution was precipitated in *n*-hexane (for $PCL_{2\ kDa}$ derivatives) and diethyl ether (for $PCL_{1.25\ kDa}$ derivatives), and the precipitated pellet was dried in vacuo. The pellet was dissolved and stirred in DMSO (10 mL) for 30 min and then was mixed with deionized water (DIW, 10 mL). The copolymer-containing mixtures in a cosolvent of DMSO and DIW were sonicated for 3 h and then were centrifuged at 4000 rpm for 20 min. The supernatant was dialyzed against DIW using a dialysis membrane (molecular weight cut-off (MWCO) of 2 or 3.5 kDa) for 24 h. The remnant solution in the membrane was lyophilized to obtain the resulting TPCL polymers with 50%–70% yields.

After dissolving the synthesized TPCL polymers in $CDCl_3$, their synthesis and chemical structure were confirmed by a 500 MHz Bruker ^{1}H-NMR spectrometer (Billerica, MA, USA): δ 1.3–1.7 (—C(=O)OCH$_2$C**H$_2$**C**H$_2$**CH$_2$C(=O)O— in the PCL backbone and $(C_6H_5)_3$-P$^+$CH$_2$C**H$_2$**C**H$_2$**CH$_2$C(=O)O— in the TPP moiety), δ 2.2–2.4 (—C(=O)OCH$_2$CH$_2$CH$_2$CH$_2$C**H$_2$**C(=O)O— in the PCL backbone and $(C_6H_5)_3$–P$^+$CH$_2$CH$_2$CH$_2$C**H$_2$**C(=O)O— in the TPP moiety), δ 3.6–3.7 (—C(=O)OCH$_2$C**H$_2$**O C**H$_2$**CH$_2$OC(=O)— in the PCL backbone and $(C_6H_5)_3$-P$^+$C**H$_2$**CH$_2$CH$_2$CH$_2$C(=O)O— in the TPP moiety), δ 4.0–4.1 (—C(=O)OC**H$_2$**CH$_2$CH$_2$CH$_2$CH$_2$C(=O)O— in the PCL backbone), δ 4.2–4.3 (—C(=O)OC**H$_2$**CH$_2$OCH$_2$C**H$_2$**OC(=O)— in the PCL backbone), and δ 7.6–7.9 ((C$_6$**H$_5$**)$_3$-**P$^+$**- in the TPP moiety).

In addition, after dissolving the synthesized polymers in DMSO, the existence of TPP moieties was further confirmed by UV/visible spectra monitored by a microplate reader (SpectraMax M5, Molecular Devices, Sunnyvale, CA) in the range of 200–300 nm and the contents of the TPP moieties were estimated by a concentration (CONC)-absorbance (ABS) standard curve of TPP^+–$COOH{\cdot}Br^-$ in DMSO at 267 nm ($CONC_{TPP\text{-}COOH\cdot Br}$ (μg mL^{-1}) = 123.27 $ABS_{TPP\text{-}COOH\cdot Br}$ − 0.9906 ($r^2 \approx 0.9998$)).

Preparation and Physicochemical Characterization of Self-Assembled TPCL Nanoparticles (NPs): In this study, self-assembled TPCL NPs were prepared from TPCL polymers using two different methods. The first method was a cosolvent dispersion (CD). Simply, after dissolving either TPP-$PCL_{1.25\ kDa}$-TPP (TPCL1) or TPP-$PCL_{2\ kDa}$-TPP (TPCL2) (5 mg) in DMSO (0.25 mL) for 30 min, DIW (7.5 mL) was poured into the polymer solution and then stirred for 10 min. The formed self-assembled NPs (i.e., TPCL1-CD NPs or TPCL2-CD NPs, respectively) in the aqueous dispersion were purified by ultrafiltration using an Amicon Ultra-15 centrifugal filter (MWCO 10 kDa) at 4000 rpm for 5 min, and the step was repeated four times. The second method was film hydration (FH). Briefly, either TPCL1 or TPCL2 (1 mg) was dissolved in chloroform (1 mL) and then the dried polymer film was prepared by evaporating the solvent. After adding DIW (2 mL) to the polymer film, the formed self-assembled NPs (i.e., TPCL1-FH NPs or TPCL2-FH NPs, respectively) in the aqueous dispersion were size-homogenized by sonication for 1 h and then additionally by extrusion at least ten times using a mini-extruder (Avanti Polar Lipid, Alabama, USA) to obtain their small and homogenous size distribution.[31]

The zeta-potentials and particle sizes of the formed TPCL-CD NPs (1 mL, 1 mg mL^{-1}) and TPCL-FH NPs (1 mL, 0.5 mg mL^{-1}) were measured with a zeta-potential and particle size analyzer (ELS-Z; Photal Otsuka Electronics Co., Osaka, Japan) with a fixed wavelength of 677 nm and a constant angle of 90° at RT.

Morphological Evaluation of TPCL NPs: To evaluate the morphology of TPCL NPs, cryo-TEM experiments were performed with a thin film of the NP solution (4 μL, 0.5 mg mL^{-1}) transferred onto a lacey supported grid. The thin aqueous films were prepared at ambient temperature at a humidity of 97%–99% within a custom-built environmental chamber to prevent the evaporation of water from the sample solution. The excess liquid was blotted with filter paper for 2–3 s, and the thin aqueous films were rapidly vitrified by plunging them into liquid ethane (cooled by

liquid nitrogen) at its freezing point. The prepared samples of NPs were transferred to a Gatan 626 cryo holder. The samples were observed using a JEM-3010 HR at liquid nitrogen temperature to prevent sublimation with a 120 kV accelerating voltage, and images were acquired with an SC 1000 CCD camera (Gatan, Inc.; Warrendale, PA).

Preparation and Physicochemical Characterization of Drug-Loaded TPCL NPs: In this study, hydrophilic doxorubicin hydrochloride (Dox·HCl) and its salt-free hydrophobic form doxorubicin (Dox) were selected as model drugs. In DMSO, Dox·HCl (20 mg mL^{-1}) was reacted with TEA (two equivalent moles of Dox·HCl) overnight and then prepared with hydrophobic Dox.

During the preparation of TPCL NPs, Dox loading was performed simultaneously. For Dox-TPCL-CD NPs, TPCL (8 mg) and Dox (2 mg) were separately dissolved in 0.4 mL and 0.1 mL of DMSO, respectively, and then two solutions were mixed and stirred for 4 h. After adding DIW (15 mL) into the mixed solution (0.5 mL) of TPCL and Dox, the solution was stirred for 10 min to form drug-loaded self-assembled NPs (i.e., Dox-TPCL1-CD NPs and Dox-TPCL2-CD NPs) in a water-rich environment. Under dark conditions, the formed Dox-TPCL-CD NPs in the aqueous dispersion were purified by ultrafiltration using an Amicon Ultra-15 centrifugal filter (MWCO 10 kDa) at 4000 rpm for 10 min, and this step was repeated four times. For Dox-TPCL-FH NPs, 0.05 mL of Dox (20 mg mL^{-1}) in DMSO was added into TPCL (4 mg) solution in chloroform (1 mL). The cosolvent was evaporated to form the dried polymer film. After adding DIW (10 mL) to the polymer film, the formed self-assembled NPs (i.e., TPCL1-FH NPs or TPCL2-FH NPs, respectively) in the aqueous dispersion were size-homogenized by sonication for 3 h at 60 °C and then additionally were filtered by a syringe filter (0.45 μm) to remove micrometer-sized particles. Under dark conditions, the formed Dox-TPCL-FH NPs in the aqueous dispersion were purified by ultrafiltration using an Amicon Ultra-15 centrifugal filter (MWCO 10 kDa) at 4000 rpm for 10 min and this step was repeated four times.

For Dox·HCl-loaded TPCL NPs, after constructing either TPCL-CD NPs or TPCL-FH NPs, Dox·HCl was remotely loaded into the NPs. When making TPCL NPs, aqueous AS solution (200×10^{-3} M) was poured into either TPCL solution in DMSO or the dried polymer film, and AS-loaded TPCL NPs were dialyzed against DIW using a dialysis membrane (MWCO 1 kDa) for 12 h to remove unloaded AS. Next, Dox·HCl (1 mg) dissolved in DIW (0.2 mL) was added into AS-loaded TPCL NP solution, and then the mixed solution was stirred overnight in water bath at 60 °C. Then, Dox·HCl-loaded TPCL NPs were purified by ultrafiltration in DIW to remove the unloaded Dox·HCl.

The particle sizes and zeta-potentials of the drug-loaded NPs were evaluated by a zeta-potential and particle size analyzer (ELS-Z; Photal Otsuka Electronics Co., Osaka, Japan) with a fixed wavelength of 677 nm and a constant angle of 90° at RT.

To evaluate DLC and DLE of drug-loaded TPCL NPs, the NPs were lyophilized and then dissolved in DMSO. After monitoring the absorbance of drugs loaded in the NPs at 485 nm with a microplate reader (SpectraMax M5, Molecular devices, Sunnyvale, CA), their concentrations were estimated with a concentration (CONC)-absorbance (ABS) standard curve of Dox·HCl prepared in DMSO ($CONC_{Dox\cdot HCl}$ (μg mL^{-1}) = $208.81ABS_{Dox\cdot HCl} + 0.2871$ ($r^2 \approx 0.9999$)). DLC and DLE were calculated by equations

$$DLC(wt\%) = \frac{\text{Weight of drug loaded in nanoparticles}}{\text{Weight of drug-loaded nanoparticles}} \times 100 \quad (1)$$

$$DLE(\%) = \frac{\text{Weight of drug loaded in nanoparticles}}{\text{Weight of drug in feed}} \times 100 \quad (2)$$

Drug Release of Drug-Loaded TPCL NPs: To monitor the release of Dox·HCl from Dox·HCl-loaded TPCL NPs, one mL of the NPs with [Dox] = 10 μg mL^{-1} was transferred into a Slide-A-Lyzer MINI dialysis device (MWCO 3.5 kDa), and DIW (4 mL) was added into a receiver. Then, the release experiments were performed at 80 rpm and 37 °C. At predetermined time points, the solution in the receiver was replaced with fresh DIW (4 mL), and the dialysate was lyophilized. After the lyophilized powder was dissolved in DMSO, the Dox·HCl concentration was calculated by observing its fluorescence at 479 nm (excitation) and 593 nm (emission).

For the NR release from NR-loaded TPCL NPs, 200 μL of the NPs with [Dox] = 10 μg mL^{-1} were transferred into a 96 well-plate and the fluorescence of NR was monitored at 552 nm (excitation) and 636 nm (emission). The NR release (%) was calculated using equation

$$\%\text{NR release} = \left(1 - \frac{\text{Fluorescence}_t}{\text{Fluorescence}_{t=0}}\right) \times 100\% \quad (3)$$

In Vitro Cytotoxicity and Antitumor Effects of Drug-Free TPCL NPs and Drug-Loaded TPCL NPs: Using a well-known MTT assay, the material cytotoxicity of drug-free TPCL-based NPs and in vitro antitumor effects of drug-loaded TPCL-based NPs were evaluated in HeLa (human cervical adenocarcinoma cell line) and HepG2 cells (human hepatoma cell lines). HeLa and HepG2 cells were cultured in RPMI-1640 and DMEM, respectively, supplemented with 10% FBS and D-glucose (2 g L^{-1} for RPMI-1640 and 4.5 g L^{-1} for DMEM) under humidified air with 5% CO_2 at 37 °C. The cells were seeded in 96-well plates at a density of 5000 cells per a well in culture medium (0.1 mL) and were incubated for 24 h. After adding drugs or NPs to the cells, the cells were incubated for 48 h, and then MTT solution (10 μL, 5 mg mL^{-1}) was added to the cells. After an additional 4 h incubation, the MTT-containing culture medium was discarded and DMSO (100 μL) was added to dissolve the formazan crystals produced by live cells. The absorbance (ABS) of the formazan was measured at 570 nm using a microplate reader (SpectraMax M5; Molecular Devices, Sunnyvale, CA) and used to calculate the viability of drug-treated or NP-treated cells with equation

$$\text{Cell viability}(\%) = \frac{ABS_{\text{sample-treated cells}} - ABS_{DMSO}}{ABS_{\text{untreated cells}} - ABS_{DMSO}} \times 100 \quad (4)$$

Cellular Uptake, Nuclear Uptake, Mitochondrial Uptake, and Intracellular Trafficking of Drug-Loaded TPCL NPs: To assess cellular uptake, nuclear uptake, and mitochondrial uptake of free drugs or drug-loaded TPCL NPs, the cells were seeded in 6-well plates at a density of 5×10^5 cells per a well in the culture medium (2 mL) and were incubated for 24 h. After a 4 h treatment with free drugs and drug-loaded TPCL NPs ([drug] = 5 μg mL^{-1}), the cells were rinsed twice with DPBS and detached. For the cellular uptake of drug-loaded TPCL NPs, cellular Dox fluorescence was measured using a flow cytometer (FACScanto II, Becton–Dickinson, Franklin Lakes, NJ, USA) with a primary argon laser (532 nm) and a fluorescence detector (578 ± 15 nm). The Dox or Dox·HCl uptake in the cells was analyzed from a gated viable population of at least 1×10^4 cells. To compare the cellular uptake of samples (i.e., free drugs and drug-loaded NPs), the normalized cellular uptake was calculated from equation

$$\text{Normalized cellular uptake of sample} = \frac{\text{Cellular uptake of sample}}{\text{Cellular uptake of free Dox·HCl}} \quad (5)$$

For nuclear uptake and mitochondrial uptake of free drugs or drug-loaded TPCL NPs, after the cells were prepared and exposed to free drugs or drug-loaded TPCL NPs as per the experiment procedure for cellular uptake, the cells were rinsed twice with DPBS and detached. Then, the samples for nuclear uptake and mitochondrial uptake of drug-loaded TPCL NPs were prepared per the protocols of the Nuclei PURE Prep nuclei isolation kit and mitochondria isolation kit, respectively. Nuclear and mitochondrial drug fluorescence was measured using a flow cytometer (FACScanto II, Becton Dickinson, Franklin Lakes, NJ, USA) with a primary argon laser (532 nm) and a fluorescence

detector (578 ± 15 nm). The normalized nuclear uptake, normalized mitochondrial uptake, and mitochondrial preference versus the nucleus were estimated with equations

$$\text{Normalized nuclear uptake of sample} = \frac{\text{Nuclear uptake of sample}}{\text{Nuclear uptake of free Dox}\cdot\text{HCl}} \quad (6)$$

$$\text{Normalized mitochondrial uptake of sample} = \frac{\text{Mitochondrial uptake of sample}}{\text{Mitochondrial uptake of free Dox}\cdot\text{HCl}} \quad (7)$$

$$\text{Mitochondrial preference to the nucleus} = \frac{\text{Normalized mitochondrial uptake of sample}}{\text{Normalized nuclear uptake of sample}} \quad (8)$$

To measure the intracellular localization and intracellular intensity of drugs delivered with drug-loaded TPCL NPs ([drug] = 1 μg mL^{-1}), the cells (3×10^4 cells per a well) were seeded in a confocal dish and incubated for 24 h. Before treatment with drug-loaded TPCL NPs, the culture medium was replaced with fresh medium (0.3 mL). After a 4 h treatment with drug-loaded TPCL NPs, the culture medium was replaced and incubated with MitoTracker Deep Red FM (150×10^{-9} M)-containing medium (0.3 mL) for 30 min. After adding Hoechst33342 (5 μg mL^{-1}) for nuclear staining in the culture medium, the cells were incubated for an additional 10 min. The cells were rinsed with DPBS for further evaluation with a laser scanning confocal microscope (LSM710; Carl Zeiss, Oberkochen, Germany) equipped with excitation lasers (408 nm for diode, 543 nm for HeNe, and 633 nm for HeNe) and variable bandpass emission filters.

Supporting Information

Supporting Information is available from the Wiley Online Library or from the author.

Acknowledgements

D.Y.C. and H.C. contributed equally to this work. This study was supported by the National Research Foundation of Korea (NRF) grants funded by the Korea government (MSIP) (Grant Nos. NRF-2012R1A1A1014718, NRF-2015R1A1A05001459, and NRF-2013R1A2A2A04015914).

Received: April 9, 2015
Revised: June 3, 2015
Published online: August 6, 2015

[1] V. P. Torchilin, *Annu. Rev. Biomed. Eng.* **2006**, *8*, 343.
[2] a) J. W. Nichols, Y. H. Bae, *Nano Today* **2012**, *7*, 606; b) L. Rajendran, H. J. Knolker, K. Simons, *Nat. Rev. Drug Discovery* **2010**, *9*, 29.
[3] M. Mossalam, A. S. Dixon, C. S. Lim, *Ther. Delivery* **2010**, *1*, 169.
[4] a) R. A. Smith, R. C. Hartley, H. M. Cocheme, M. P. Murphy, *Trends Pharmacol. Sci.* **2012**, *33*, 341; b) A. Szewczyk, L. Wojtczak, *Pharmacol. Rev.* **2002**, *54*, 101.
[5] Y. Yamada, H. Harashima, *Adv. Drug Delivery Rev.* **2008**, *60*, 1439.
[6] I. Meton, M. Egea, F. Fernandez, M. C. Eraso, I. V. Baanante, *FEBS Lett.* **2004**, *566*, 251.
[7] I. N. Shokolenko, M. F. Alexeyev, S. P. LeDoux, G. L. Wilson, *DNA Repair* **2005**, *4*, 511.
[8] K. Takaya, Y. Higuchi, K. Kitamoto, M. Arioka, *FEMS Microbiol. Lett.* **2009**, *301*, 201.
[9] N. D. Marchenko, A. Zaika, U. M. Moll, *J. Biol. Chem.* **2000**, *275*, 16202.
[10] A. L. Horwich, F. Kalousek, I. Mellman, L. E. Rosenberg, *EMBO J.* **1985**, *4*, 1129.
[11] a) G. R. Chamberlain, D. V. Tulumello, S. O. Kelley, *ACS Chem. Biol.* **2013**, *8*, 1389; b) R. Mourtada, S. B. Fonseca, S. P. Wisnovsky, M. P. Pereira, X. Wang, R. Hurren, J. Parfitt, L. Larsen, R. A. Smith, M. P. Murphy, A. D. Schimmer, S. O. Kelley, *PLoS One* **2013**, *8*, e60253.
[12] R. A. Smith, R. C. Hartley, M. P. Murphy, *Antioxid. Redox. Signal* **2011**, *15*, 3021.
[13] M. C. Frantz, P. Wipf, *Environ. Mol. Mutagen.* **2010**, *51*, 462.
[14] a) G. G. D'Souza, R. Rammohan, S. M. Cheng, V. P. Torchilin, V. Weissig, *J. Controlled Release* **2003**, *92*, 189; b) Y. Yamada, H. Akita, K. Kogure, H. Kamiya, H. Harashima, *Mitochondrion* **2007**, *7*, 63.
[15] P. G. Finichiu, A. M. James, L. Larsen, R. A. Smith, M. P. Murphy, *J. Bioenerg. Biomembr.* **2013**, *45*, 165.
[16] T. A. Theodossiou, Z. Sideratou, M. E. Katsarou, D. Tsiourvas, *Pharm. Res.* **2013**, *30*, 2832.
[17] J. Callahan, J. Kopecek, *Biomacromolecules* **2006**, *7*, 2347.
[18] J. Qiao, Z. Liu, Y. Tian, M. Wu, Z. Niu, *Chem. Commun.* **2015**, *51*, 3641.
[19] S. Marrache, S. Dhar, *Proc. Natl. Acad. Sci. USA* **2012**, *109*, 16288.
[20] P. K. Avti, D. Maysinger, A. Kakkar, *Molecules* **2013**, *18*, 9531.
[21] S. Biswas, N. S. Dodwadkar, P. P. Deshpande, V. P. Torchilin, *J. Controlled Release* **2012**, *159*, 393.
[22] a) W. K. Oh, S. Kim, H. Yoon, J. Jang, *Small* **2010**, *6*, 872; b) S. Cai, K. Vijayan, D. Cheng, E. M. Lima, D. E. Discher, *Pharm. Res.* **2007**, *24*, 2099.
[23] D. E. Discher, V. Ortiz, G. Srinivas, M. L. Klein, Y. Kim, D. Christian, S. Cai, P. Photos, F. Ahmed, *Prog. Polym. Sci.* **2007**, *32*, 838.
[24] M. Millard, D. Pathania, Y. Shabaik, L. Taheri, J. Deng, N. Neamati, *PLoS One* **2010**, *5*, e13131.
[25] M. A. Solomon, A. A. Shah, G. G. D'Souza, *Mitochondrion* **2013**, *13*, 464.
[26] P. Yu, H. Yu, C. Guo, Z. Cui, X. Chen, Q. Yin, P. Zhang, X. Yang, H. Cui, Y. Li, *Acta Biomater.* **2015**, *14*, 115.
[27] a) S. Zhang, J. Li, G. Lykotrafitis, G. Bao, S. Suresh, *Adv. Mater.* **2009**, *21*, 419; b) A. Xu, M. Yao, G. Xu, J. Ying, W. Ma, B. Li, Y. Jin, *Int. J. Nanomed.* **2012**, *7*, 3547.
[28] a) H. C. Kang, O. Samsonova, Y. H. Bae, *Biomaterials* **2010**, *31*, 3071; b) V. A. Sethuraman, K. Na, Y. H. Bae, *Biomacromolecules* **2006**, *7*, 64; c) D. Mishra, H. C. Kang, Y. H. Bae, *Biomaterials* **2011**, *32*, 3845.
[29] a) Y. Li, X. Chen, N. Gu, *J. Phys. Chem. B* **2008**, *112*, 16647; b) K. Kobayashi, J. Wei, R. Iida, K. Ijiro, K. Niikura, *Polym. J.* **2014**, *46*, 460.
[30] a) J. A. Champion, S. Mitragotri, *Proc. Natl. Acad. Sci. USA* **2006**, *103*, 4930; b) J. A. Champion, S. Mitragotri, *Pharm. Res.* **2009**, *26*, 244.
[31] S. S. Malhi, A. Budhiraja, S. Arora, K. R. Chaudhari, K. Nepali, R. Kumar, H. Sohi, R. S. Murthy, *Int. J. Pharm.* **2012**, *432*, 63.